I&EC research
Industrial & Engineering Chemistry Research

Article

Cite This: Ind. Eng. Chem. Res. 2018, 57, 3246−3254

pubs.acs.org/IECR

Magnetic-Field-Induced Deformation Analysis of Magnetoactive Elastomer Film by Means of DIC, LDV, and FEM

Jiabin Feng, Shouhu Xuan,* Zeqian Lv, Lei Pei, Qingchuan Zhang, and Xinglong Gong*

CAS Key Laboratory of Mechanical Behavior and Design of Materials, Department of Modern Mechanics, University of Science and Technology of China, Hefei 230027, People's Republic of China

Supporting Information

ABSTRACT: This work studied a flexible and stretchable magnetoactive elastomer (MAE) film consisting of carbonyl iron (CI) particles and polydimethylsiloxane (PDMS) elastomer matrix. The deformation of the MAE film was investigated using digital image correlation (DIC) and laser Doppler velocimetry (LDV) methods. The MAE film with free boundary is highly wrinkled under a magnetic field generated by an electromagnet with the current of 0.65 A. While in fixed boundary condition, the maximum deformation appears at the center point, and the maximum displacement reaches 0.63 mm when the current is 3 A. The finite element method (FEM) results demonstrate that the maximum internal stress and strain are 33 kPa and 2.3%, respectively. The FEM results are in good agreement with the DIC and LDV tests. With the exceptional magnetic controllability, the MAE film can find extensive applications in intelligent control systems, acoustic absorption devices, and haptics.

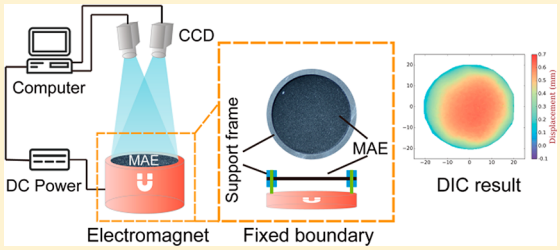

1. INTRODUCTION

Magnetoactive materials have drawn more and more attention due to their specific abilities to realize intelligent control.[1,2] Among them, the magnetoactive elastomer (MAE) is a potential prospect for the realization of magnetic manipulation.[3] The MAE mainly consists of magnetic particles and a soft elastomer matrix.[4] The embedded magnetic particles are dispersed isotropically or anisotropically in the soft elastomer matrix.[5] The mechanical properties of MAE can be controlled by the magnetic field, as the magnetic force can be imposed on the magnetic particles.[6] Recently, researchers have developed a new kind of MAE, named as a MAE film, by decreasing the thickness of MAE.[7,8] The MAE film shows good magnetic controllability, flexibility, and stretchability.[9] To this end, the MAE film can be widely employed in diverse functional devices, such as the actuators,[10] inductors,[11] soft platforms,[12] tunable interfaces,[13] adhesives,[14] etc.

To further understand the mechanical properties of the MAE film, many researchers focus on the magnetic-field-induced deformation.[15,16] Rudykh et al. investigated the stability of magnetorheological elastomers suffering from finite deformations. The results reveal that instabilities are promoted when the magnetic field is perpendicular to the layers.[17] Meanwhile, Danas et al. studied the instability of a magnetoelastic layer resting on a nonmagnetic substrate.[18] When subjected to transverse magnetic fields, the magnetoactive elastomers become frilly. The controllable surface roughness of the MAE film is attractive in haptics. More interestingly, the MAE membrane with tunable effective mass density has been applied in sound isolation.[19] The resonant frequency of the structured MAE is actively tunable by external gradient magnetic field. Although the magnetic-field-induced deformation has been preliminarily studied, the detailed mechanism is still mysterious. Moreover, the influence of the fixing boundary condition on the magnetic-field-induced deformation of the MAE film has not been experimentally investigated.

The traditional approaches are not proper to measure the deformation of the MAE film because of its good flexibility and stretchability.[20] The digital image correlation (DIC) method is a far-field measurement without complex optical path,[21] and thus it becomes an exceptional methodology for full-field deformation measurements.[22,23] The camera used in the DIC test is not a high-speed camera, which limits the utilization in transient deformation measurements. To overcome this shortcoming, laser Doppler velocimetry (LDV) technology is employed to investigate the transient deformation of the MAE film under different magnetic fields. The LDV technology is an impressive method to measure the deformation even at high change rate.[24] However, some properties of the deformed MAE film are difficult to be measured by experiment. Fortunately, numerical methods, such as the finite element method (FEM), have proven to be a reliable way to calculate the particular properties of MAE.[25,26] Based on the above analysis, the combination of the DIC, LDV, and FEM methods to study the deformation of MAE film is anticipated.

Herein, we fabricated an MAE film composed of CI particles and PDMS elastomer matrix. The MAE film was placed on the top of an electromagnet with free or fixed boundary. The influence of magnetic field on the deformations of the MAE

Received: November 24, 2017
Revised: February 6, 2018
Accepted: February 12, 2018
Published: February 12, 2018

DOI: 10.1021/acs.iecr.7b04873
Ind. Eng. Chem. Res. 2018, 57, 3246−3254

film was measured by using DIC and LDV methods. The full-field deformation was achieved by DIC and the detailed deformation evolution was obtained by LDV. Meanwhile, some particular properties, such as the internal stress and strain, were calculated by FEM. Finally, the MAE film with good magnetic controllability, flexibility, and stretchability can be utilized in magnetic actuation and sound absorption.

2. MATERIALS AND METHODS

2.1. Materials. The carbonyl iron (CI) particles were provided by BASF in Germany. The average size of CI particles is 7 μm. The polydimethylsiloxane (PDMS) precursor and curing agent (Sylgard 184) were obtained from Dow Corning. The CI particles and PDMS were used as the magnetic filler and matrix of magnetoactive elastomer (MAE), respectively.

2.2. Preparation. A total of 4.4 g of CI particles and 0.4 g of PDMS curing agent were added into 4 g of PDMS precursor. The mixture was mechanically stirred for 10 min. Then, the mixture was sonicated for 10 min to make the CI particles well dispersed. The mixture was degassed in a vacuum container for 20 min to remove the trapped bubbles. After that, the mixture was poured on the surface of a silicon wafer. The silicon wafer was placed on the center surface of a spin coater. The MAE mixture was spin coated at 1000 rpm for 60 s and cured at 100 °C for 10 min. The resulting MAE film was released from the silicon wafer by manual peeling (Figure 1).

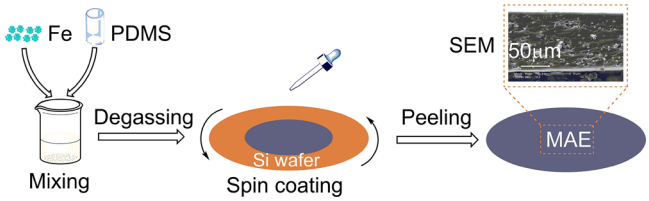

Figure 1. Schematic illustrations of MAE film preparation.

2.3. Characterization. A scanning electron microscope (SEM, XT30 ESEM-MP, Philips of Holland) was used to observe the microstructure of the MAE film. The accelerating voltage was 20 kV. The uniaxial tension test was carried out by a universal testing machine (RGM 6005T, Shenzhen REGER Instrument Co., Ltd.). The MAE film was cut into a dumbbell shape. The length and width of the test section of the MAE film were 10 and 4 mm, respectively. The tensile velocity was set as 20 mm/min.[27] Meanwhile, the storage modulus was measured by using a rheometer (Physica MCR 301, Anton Paar).

Furthermore, the digital image correlation (DIC) method was employed to investigate the magnetic-field-induced deformation of the MAE film (Figure 2a). Two cameras with proper angles were used to take photos of the specimen for calculating the deformation. In the DIC test, the pixel was 2048 × 2048 and the sampling frequency was 8 Hz. A round MAE film was hung over an electromagnet with free and fixed boundary (Figure 2b,c). For the electromagnet, the outer and inner diameters of the coil were 95 and 52 mm, respectively. The height of the coil was 60 mm. The diameter of the MAE film was 50 mm, and the distance between the MAE film and electromagnet was 4 mm. When the current in the electromagnet was 1, 2, and 3 A, the measured magnetic fields at the center of the MAE film surface were 36, 71, and 106 mT, respectively. A kind of white paint was sprinkled on the surface of MAE film to form the speckle pattern. In the free boundary

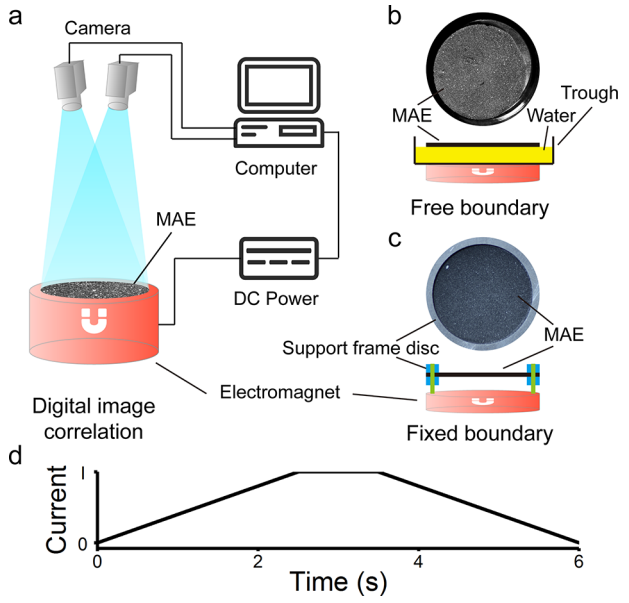

Figure 2. (a) Schematic illustration of the digital image correlation (DIC) method. The photograph of the MAE film and corresponding fixed structure with (b) free boundary and (c) fixed boundary. (d) The current−time curve of the input current of the electromagnet in the DIC experiment.

condition, the MAE film was floated on the surface of the water in a round trough, so the MAE film could deform freely (Figure 2b). In the case of fixed boundary condition, the MAE film was fixed on a support frame disc which had a hole at the center with a diameter of 42 mm (Figure 2c). Thus, the edge part of MAE film was fixed on the support frame disc, but the center part of MAE film with a diameter of 42 mm could deform freely. Then, the disc, as well as the round MAE film, was fixed on the top of the electromagnet. A programmable power supply (IT6724, ITECH Co., Ltd.) was used to produce a trapezoidal current (Figure 2d). The maximum current in the free boundary test was 0.65A, while that in the fixed boundary experiment was 1, 2, and 3 A. All of the capturing and analysis processes were carried out by a commercial DIC analyzer (PMLAB DIC-3D, Nanjing PMLAB Sensor Tech. Co., Ltd.).

As the sampling rate of the DIC method is not very high, it is hard to obtain the transient deformation of the MAE film when a magnetic field is suddenly applied. Thus, we utilized LDV to study the transient deformation of the MAE film by using a laser Doppler vibrometer (PSV-400-M2, Polytec Co., Ltd.; Figure 3a). The laser Doppler vibrometer could only measure one point at a time, and the sampling frequency of LDV was 256 Hz. Thus, only the transient deformation of the MAE film with fixed boundary was presented due to the symmetry of the structure (Figure 3b). However, it is difficult to measure all of the points on the surface of MAE film. For simplicity, only 21 points were chosen for deformation representation (Figure 3c). These 21 points were located at the intersection of multiple concentric circles and coordinate axes (Figure 3c). The radii of multiple concentric circles were 0, 3.5, 7.0, 10.5, 14.0, and 17.5 mm. The deformation at the radius of 21 mm was considered to be zero. For accurate comparison, the surface out-of-plane displacement was chosen to represent the deformation state of the MAE film under applying the external magnetic field. Alternatively, a square wave was selected as the input current to investigate the transient deformation of the MAE film induced

DOI: 10.1021/acs.iecr.7b04873
Ind. Eng. Chem. Res. 2018, 57, 3246−3254

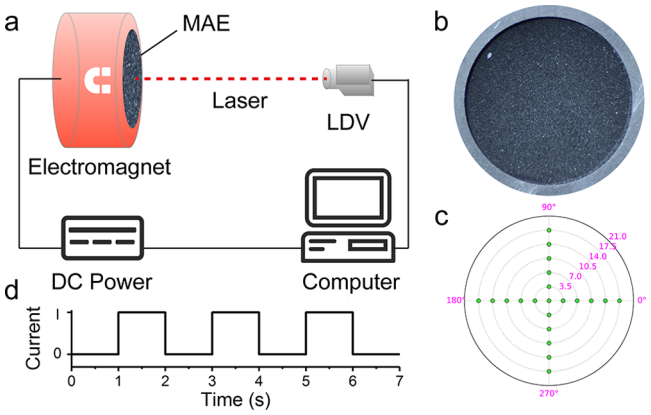

Figure 3. (a) Schematic illustration of the LDV test. (b) Photograph of MAE film with fixed boundary. (c) Schematic illustration of the distribution of the measuring points. (d) The current−time curve of the input current of the electromagnet in the LDV test.

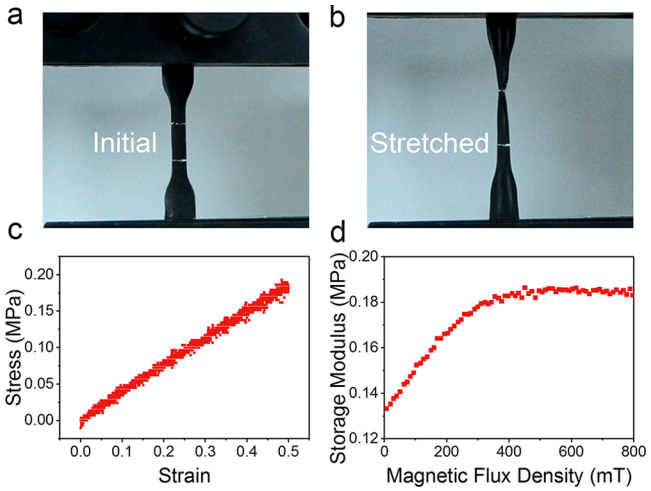

Figure 4. Photograph of the dumbbell-shaped MAE film at (a) initial and (b) stretched state. (c) The stress−strain curve of the MAE film. (d) The storage modulus versus the magnetic flux density.

by step current (Figure 3d). The current first turned off for 1 s and then turned on for the next 1 s and this process was repeated with a periodic time of 2 s. Thus, the frequency of the current can be considered as 0.5 Hz. The amplitude of the current was set as 1, 2, and 3 A. All of the tests were repeated at least three times.

2.4. Numerical Methods. The finite element method (FEM) was employed to calculate the internal stress and strain of the MAE film, which was difficult to be measured by using experimental methods.[28] The simulation was carried out by Ansoft Maxwell and ANSYS Workbench. The geometry was directly established in Ansoft Maxwell 3D. The solids included the MAE film, copper coil, iron core, and air region. Each solid was endowed with the corresponding material properties. Current excitations were added to the copper coil. The inside selection was chosen as the mesh operation. Then, the magnetic field distribution can be calculated. After that, the geometry and solution were transferred to ANSYS Workbench. The material properties of the MAE film were added in engineering data. A fixed support was applied to the edge of the MAE film. The force acting on the MAE film was imported from Ansoft Maxwell 3D Solution. After proper meshing, the deformation, stress, and strain of the MAE film can be obtained by solving the project.

3. RESULTS AND DISCUSSION

3.1. Characterization of the MAE Film. The SEM analysis demonstrates that the CI particles are randomly dispersed in a PDMS matrix (Figure 1). The combination between CI particles and PDMS is strong. The average thickness of the MAE film is nearly 100 μm. Meanwhile, a uniaxial tension test was employed to study the stretchability of the MAE film. At the initial state, the MAE film is in a dumbbell shape, and its surface is flat (Figure 4a). After stretching, the MAE film is elongated and finally fractures when the maximum strain is reached (Figure 4b). Figure 4c shows the strain−stress curve of the MAE film. When the applied strain is lower than 50%, the tensile stress is nearly linear with the applied strain. The MAE film is fractured while the applied strain exceeds 50%. The maximum tensile strength of the MAE film is 0.19 MPa, and the Young's modulus of the MAE film is 0.38 MPa. The experimental results demonstrate that the MAE film has low Young's modulus and exhibits good stretchability. Meanwhile, the storage modulus at the presence of a magnetic field is shown in Figure 4d. The storage modulus increases with the increasing of magnetic field and reaches equilibrium when the magnetic field exceeds 400 mT. Therefore, the stiffness of the MAE film can be controlled by the external magnetic field.

3.2. Magnetic-Field-Induced Deformation of the MAE Film with Free Boundary. As mentioned above, the MAE film consists of CI particles and a PDMS matrix. As the CI particles are soft magnetic materials, they can be easily magnetized by the external magnetic field. The magnetic dipole moment $\vec{m}$ between two nearby magnetized CI particles is given by[29]

$$3\hat{n}\hat{n}\cdot\vec{m} - \vec{m} = \frac{4\pi r^3}{\mu_0}\vec{B}, \quad r > 0 \tag{1}$$

where the r is the radius of the magnetic particles, $\hat{n}$ is the unit vector of $\hat{r}$, μ_0 is the permeability of vacuum, and $\vec{B}$ is the magnetic flux density. A kind of force can be generated on the magnetic dipole when they are in gradient magnetic field. The force is given by[29]

$$\vec{F} = \nabla(\vec{m}\cdot\vec{B}) \tag{2}$$

Then, the magnetic dipoles can be forced to move by the external gradient magnetic field. Meanwhile, the magnetic dipoles can drive the MAE film to deform due to the low stiffness of the MAE film. The full-field deformation of the MAE film with free boundary is presented in Figure 5. The sag direction is the positive direction. At the initial state, the MAE film is flat and no deformation appears. With increasing of the current in the electromagnet, a crescent area at the edge begins to sag. As the current raises to 0.65 A at 2.5 s, the sag displacement reaches a maximum of 1.75 mm. Then, the deformation stays the same when the current is kept constant at 0.65 A from time 2.5 to 3.5 s. After that, the MAE film recovers to the initial state as the current decreases to 0 A from time 3.5 to 6 s (Movie S1).

To better understand the detailed deformation, the displacement curves of the six feature points at different regions are presented in Figure 6. Points 1−4 form a straight line. Points 5 and 6 are nearly symmetrically distributed on both sides of the line (Figure 6a). For all six feature points, the displacement first

DOI: 10.1021/acs.iecr.7b04873
Ind. Eng. Chem. Res. 2018, 57, 3246−3254

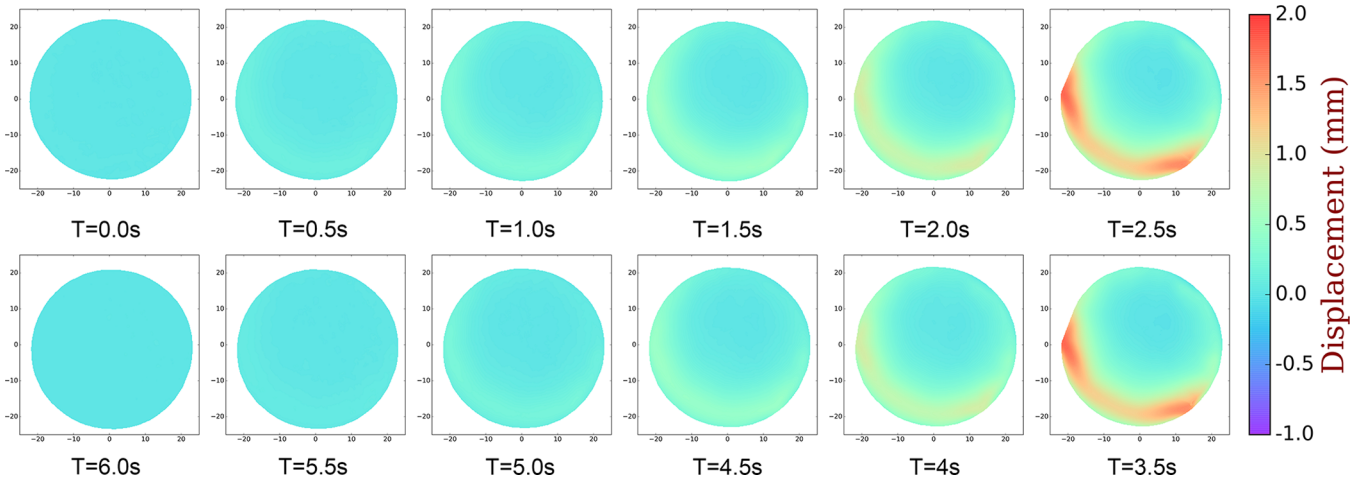

Figure 5. Magnetic-field-induced deformation of the MAE film with free boundary when the time varies from 0.0 to 6.0 s.

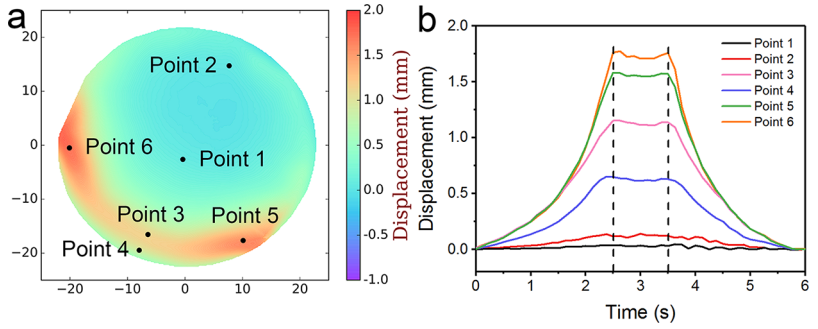

Figure 6. (a) Distribution of the six feature points. (b) The displacement curves of the six feature points.

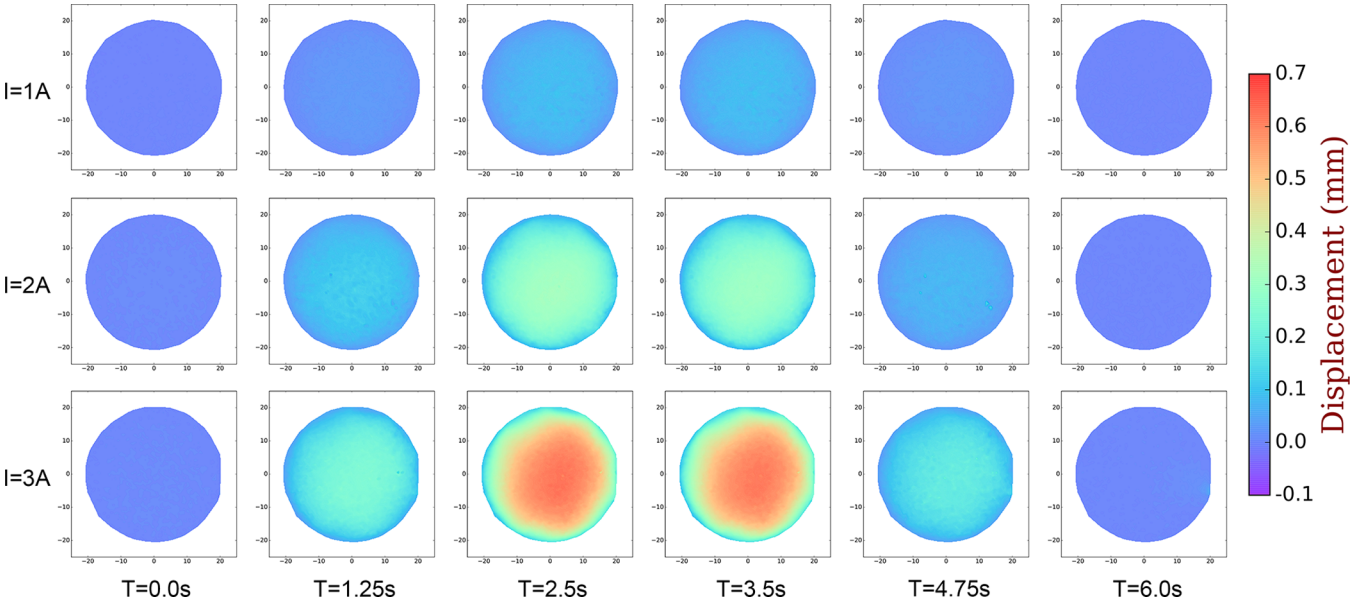

Figure 7. Magnetic-field-induced deformation of the MAE film with fixed boundary when the maximum current varies from 1, 2, to 3 A.

increases to a maximum when the time varies from 0.0 to 2.5 s and then keeps constant as the time changes from 2.5 to 3.5 s. Finally, the displacement decreases to 0 mm when the time reaches 6 s (Figure 6b). At 2.5 s, the displacement of point 1 is the smallest, while that of point 6 is the largest. The displacement of point 3 is larger than those of points 1 and 4, which means that the depression occurs at point 3. The shape of the MAE film can be easily controlled and the MAE film shows excellent magnetic-field-induced deformation properties. The MAE film exhibits good recoverability when removing the magnetic field. However, the traditional MAE cannot deform freely due to its large thickness.[5] Therefore, reducing the thickness of the MAE film can increase its flexibility and enlarge the deformation under the external

DOI: 10.1021/acs.iecr.7b04873
Ind. Eng. Chem. Res. 2018, 57, 3246−3254

magnetic field. The experimental results are consistent with the theoretical consequences pointed out by Rudykh[17] and Danas.[18]

3.3. Magnetic-Field-Induced Deformation of the MAE Film with Fixed Boundary. The deformation of the MAE film with free boundary shows randomness and asymmetry. To make the deformation more stable and symmetrical, the boundary of the MAE film was fixed on a disc. The deformations of the MAE film under different magnetic field are shown in Figure 7. Similar to the free boundary condition, the deformation first increases to a maximum at 2.5 s and then keeps constant when the time varies from 2.5 to 3.5 s. Finally, the MAE film recovers to initial state when the current decreases to 0 A at the time of 6.0 s (Movies S2, S3, and S4). Interestingly, the maximum displacement nearly occurs at the center of the MAE film, which is different from that in free boundary condition. The maximum displacements under the currents of 1, 2, and 3 A are 0.10, 0.33, and 0.63 mm, respectively. Meanwhile, the MAE film deforms like a bowl and the deformation is symmetric. For simplicity, only the displacement curves of the three feature points are demonstrated to analyze the deformation details. The three points are in a straight line. As shown in Figure 8b, the maximum

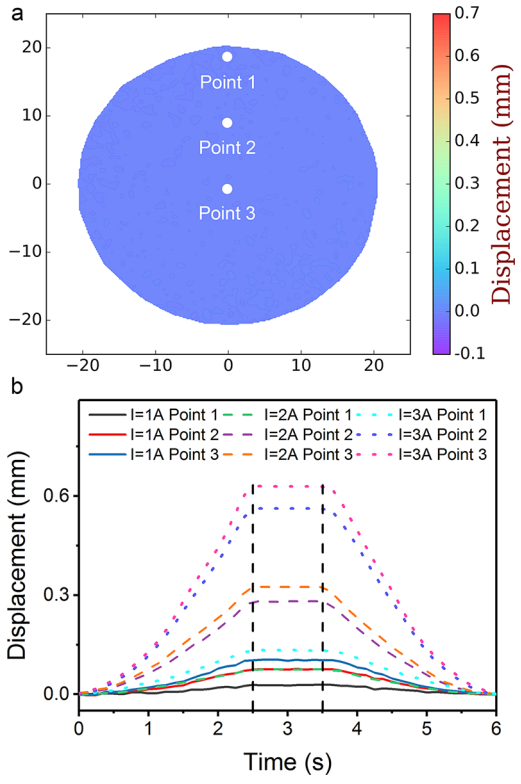

Figure 8. (a) Distribution of three feature points. (b) The displacement curves of the three feature points under different currents.

displacements under different conditions occur at time 2.5 s and keep constant for 1 s before reduction. In the same current condition, the maximum displacement increases with a variation of points from points 1 to 3. For a given point, the maximum displacement increases with the current.

However, due to the low sampling rate of the DIC method, the transient deformation of the MAE film under applying a step current can be hardly measured. Here, LDV was applied to capture the transient deformation of the MAE film. In fact, the LDV can measure the transient deformation velocity accurately. Then, the transient displacement can be obtained by integrating the velocity with time. Figure 9a demonstrates the transient deformation velocities of the center point under different currents. The current was turned off at the initial state. Then, the current was switched on at T_0, and a corresponding magnetic field was generated. The MAE film sages rapidly and the velocity drastically increases to maximum at T_1. Then, the velocity decreases to 0 mm/s at T_2. After that, the velocity becomes negative until the time reaches T_3. From T_3 to T_4, the velocity almost keeps 0 mm/s. When the current is switched off at T_4, the velocity first increases to a maximum at T_5 and then decreases to 0 mm/s at T_6 in the negative direction. The time discussed above from T_0 to T_6 is named as the characteristic time. The results demonstrate that the MAE film deforms to the stabilized state when the time changes from T_0 to T_3. The MAE film springs back to the initial state when the time varies from T_4 to T_6. Meanwhile, the characteristic time under different currents is the same. The maximum sagging velocity increases with the applied current. The transient deformation velocities of three points at 0, 10.5, and 17.5 mm under the current of 3 A are presented in Figure 9b. Interestingly, the velocity−time curves of these three points have the same shape. Meanwhile, the characteristic time at different positions is the same. The maximum sagging velocity is higher when the position is closer to the center.

The maximum sagging velocities of the whole MAE film under different currents are calculated by using the results of the 21 points measured above (Figure 10a−c). The maximum sagging velocities under different currents have the same trend. The maximum sagging velocity at the center point is larger than that at the edge. Meanwhile, the maximum sagging velocity distributions under different currents are symmetrical according to the results. To investigate the detailed distribution of the maximum sagging velocity, the maximum sagging velocities along one direction under different currents are chosen for the demonstration (Figure 10d). The maximum sagging velocity distributions under different currents are truly symmetrical apart from a few points. The maximum sagging velocities of the center point under the currents of 1, 2, and 3 A are nearly 0.62, 2.56, and 5.20 mm/s, respectively.

The deformation of the MAE film can be calculated by integrating the velocity. The deformations of the center point under different currents are demonstrated in Figure 11a. The displacement increases rapidly when the time varies from T_0 to T_2. The displacement reaches a maximum at T_2. Then, the displacement decreases to an equilibrium state when the time reaches T_3. The deformation of the MAE film remains stable as the time changes from T_3 to T_4. The displacement suddenly begins to decrease when turning off the current at T_4. Finally, the displacement changes to 0 mm and the MAE film reverts to the initial state at T_6. Interestingly, the trend of the displacement-time curves under different currents is the same and the characteristic time is also identical to each other. Moreover, the characteristic time of displacement is coinciding with that of velocity. The displacement at the equilibrium state increases with the applied current. The displacements of three points at 0, 10.5, and 17.5 mm under the current of 3 A are presented in Figure 11b. The displacement−time curves have the same trend and the characteristic time is also the same. Meanwhile, the displacement decreases with the position of the measuring point.

DOI: 10.1021/acs.iecr.7b04873
Ind. Eng. Chem. Res. 2018, 57, 3246−3254

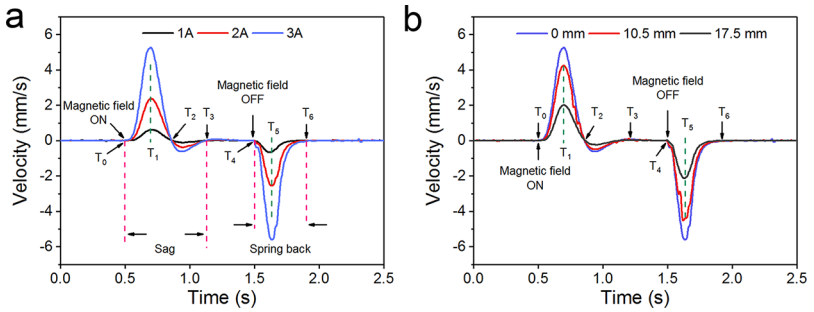

Figure 9. (a) Transient deformation velocities of the center point under the currents of 1, 2, and 3 A. (b) The transient deformation velocities of three points at the position of 0, 10.5, and 17.5 mm when the current is 3 A.

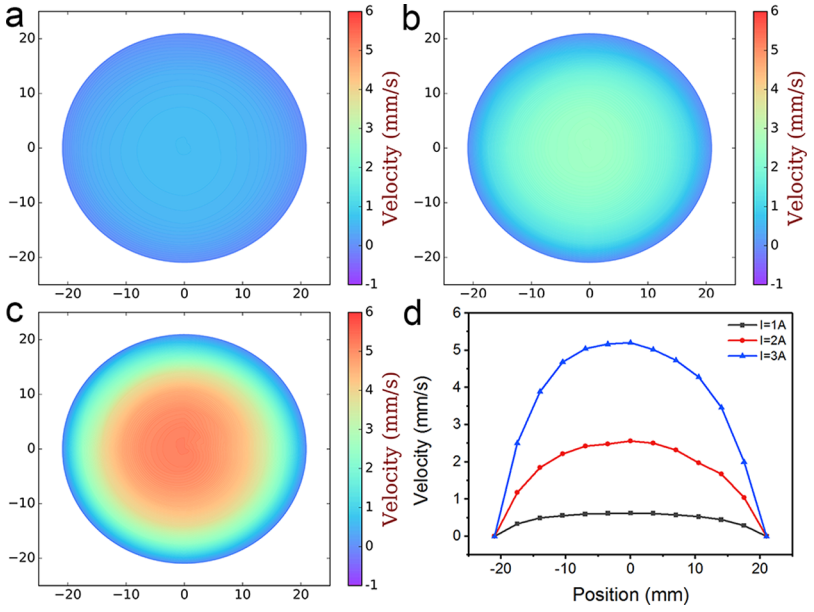

Figure 10. Maximum sagging velocities of the MAE film under the currents of (a) 1, (b) 2, and (c) 3 A. The maximum sagging velocities at the positions from −21 to +21 mm under different currents.

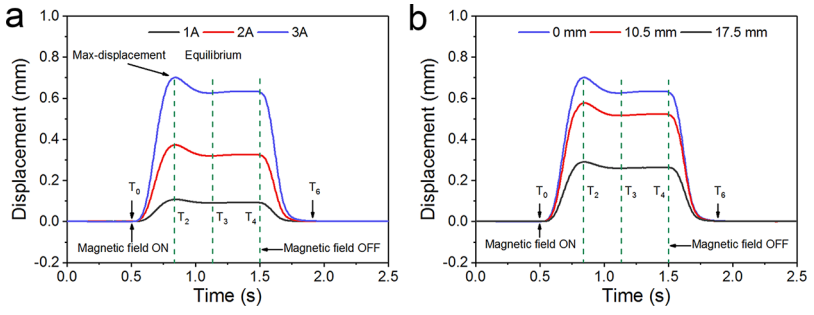

Figure 11. Final deformations of the center point under 1, 2, and 3 A. (b) The final deformations of three points at the positions of 0, 10.5, and 17.5 mm when the current is 3 A.

The displacements of the MAE film at equilibrium state under different currents are demonstrated in Figure 12a−c. When the current is 1 A, the displacement is very small. By increasing the current, the displacement begins to grow coinciding with the depression of the MAE film. The detailed deformations tested by the DIC and LDV under different currents are presented in Figure 12d. The deformation of the MAE film is symmetrical. For the LDV test, the displacements at equilibrium state of the center point under the currents of 1, 2, and 3 A are nearly 0.09, 0.33, and 0.63 mm, respectively. The results demonstrate that the deformations of the DIC test are consistent with those of LDV test under different currents.

3.4. Finite Element Simulation of the Deformation of the MAE Film with Fixed Boundary. The magnetic-field-induced deformation properties of the MAE film under different currents have been experimentally studied. However, the internal stress and strain of the MAE film still remain unknown because it is difficult to measure the internal stress and strain by using experimental methods. Thus, the finite element method (FEM) was used to calculate the internal stress and strain of the MAE film. The deformation under the

DOI: 10.1021/acs.iecr.7b04873
Ind. Eng. Chem. Res. 2018, 57, 3246−3254

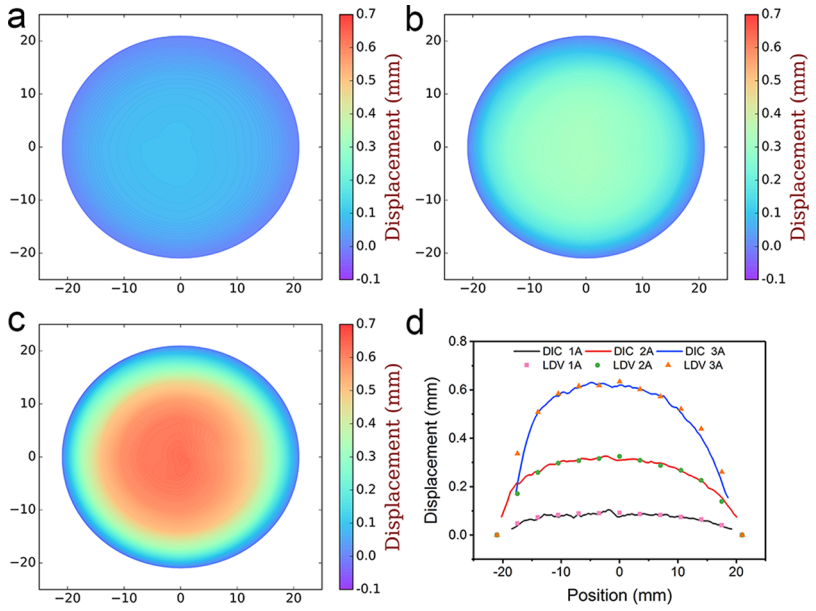

Figure 12. Final deformations of the MAE film under the currents of (a) 1, (b) 2, and (c) 3 A. The final deformations of DIC and LDV test under different currents.

current of 3 A is larger than that when the current is 2 and 1 A. The internal stress and strain reach a maximum when the current is 3 A. Therefore, in order to simplify the calculation, only the FEM results with the current of 3 A are demonstrated in the following discussion.

The magnetic field distribution of the electromagnet under the current of 3 A is shown in Figure13. The color bar data is

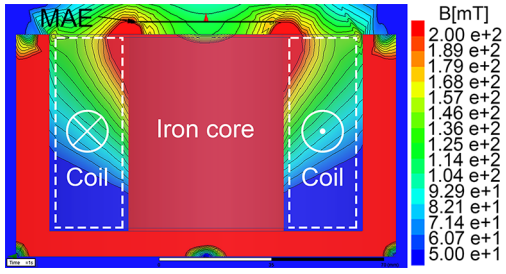

Figure 13. Detailed magnetic field distribution when the current is 3 A.

limited between 50 and 200 mT to make the magnetic field contour more readable. The magnetic field is axisymmetric. The magnetic field at the center of the MAE film is nearly 106 mT, while the magnetic field at the edge of the MAE film is nearly 164 mT. The DIC, LDV, and FEM results of the deformation of the MAE film at the current of 3 A are demonstrated in Figure 14. The displacements of the center area of the MAE film are nearly the same for the DIC, LDV, and FEM results. The FEM result agrees well with the experimental results though a little difference exists between the shape of the deformed surface of the experimental and simulation results. This difference happens because the MAE film is simplified as a two-dimensional disc in FEM as the thickness of MAE film is very small. Fortunately, this simplification is within an acceptable range and cannot cause big errors. Thus, the FEM method can be used to evaluate the particular properties which are difficult to measure by experiments, such as internal stress and strain. As shown in Figure 15a, the internal stress of the MAE film is centrosymmetric. The stress at the center point of the MAE film is nearly 22 kPa. The stress first decreases to a minimum value of 7 kPa and then increases to a maximum value of 33 kPa, when the measuring point varies from center to edge. The maximum stress happens at the edge of the MAE film. Meanwhile, the maximum stress is far less than the breaking strength of the MAE film. Interestingly, the internal strain distribution of the MAE film is also centrosymmetric, which is similar to the stress (Figure 15b). The strain at the center point of the MAE film is nearly 1.6%. The minimum and maximum strains are 0.4% and 2.3%, respectively. The

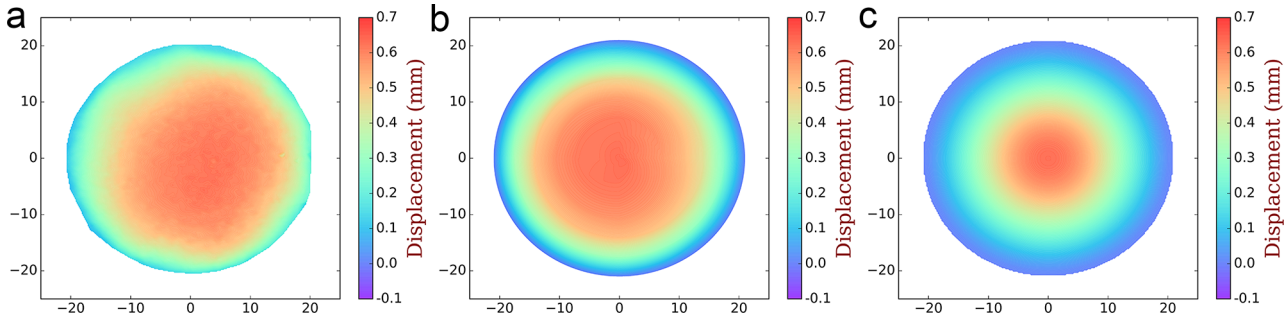

Figure 14. (a) DIC, (b) LDV, and (c) FEM results of the deformation of MAE film under the current of 3 A.

DOI: 10.1021/acs.iecr.7b04873
Ind. Eng. Chem. Res. 2018, 57, 3246−3254

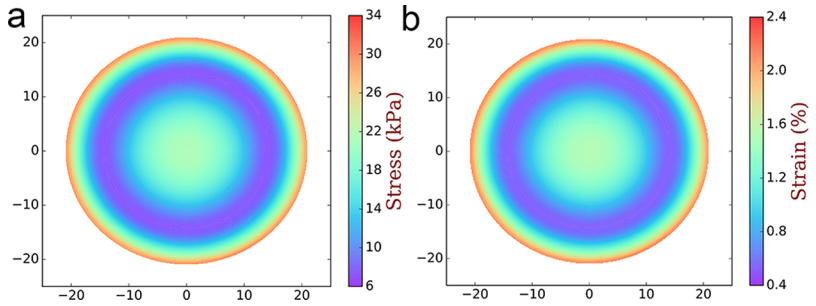

Figure 15. FEM results of the internal stress and strain.

maximum strain also occurs at the edge of the MAE film. The maximum strain is within the elastic interval and far less than the fracture strain of 50%. The FEM results demonstrate that the deformation of the MAE film is within the range of elastic deformation. Therefore, the deformation is steady and the MAE film can recover to the initial state after deformation.

Herein, the shape of the MAE film can be controlled by the external magnetic field. Meanwhile, the deformation and the external magnetic force will affect the stiffness of the MAE film. The stiffness is the main factor contributing to the resonant frequency, which determines the sound absorption property of the MAE film.[19] Therefore, due to the good magnetic controllability, flexibility, and stretchability, the MAE film is expected to be a particularly promising alternative for active sound absorption.[30]

4. CONCLUSIONS

This work reported a MAE film composed of carbonyl iron particles and a PDMS matrix. The MAE film can be stretched as large as 50%. Then, the magnetic-field-induced deformations of the MAE film with free and fixed boundary were systematically investigated by using DIC and LDV methods. Under free boundary conditions, the MAE film shows excellent magnetic-field-induced deformation properties. The maximum displacement can reach as large as 1.75 mm when the current reaches 0.65 A. The MAE film with fixed boundary deforms like a bowl, and the deformation is symmetrically distributed. The maximum displacements at the currents of 1, 2, and 3 A are 0.10, 0.33, and 0.63 mm, respectively. The transient deformations of the MAE film under different currents were investigated. The maximum deformation of the MAE film is consistent with that in the DIC test. The results demonstrate that the DIC method is a proper way for full-field deformation measurement at low deformation rate. The LDV method is suitable for the detailed deformation evolution measurement of the MAE film when the deformation rate is high. Meanwhile, according to the FEM results, the maximum stress and strain appear at the edge of the MAE film. The maximum stress and strain under the current of 3 A are 33 kPa and 2.3%, respectively. The deformation of the MAE film is within the elastic range. Thus, the FEM method can be used to evaluate the particular properties which are difficult to measure by experiment. This work may give insights into new applications in actuators, sensors, and sound absorptions.

■ ASSOCIATED CONTENT

Supporting Information

The Supporting Information is available free of charge on the ACS Publications website at DOI: 10.1021/acs.iecr.7b04873

The deformation of MAE film with free boundary when the current varies from 0A to 0.65A and back to 0A (Movie S1). (MPG)

The deformation of MAE film with fixed boundary when the current varies from 0A to 1A and back to 0A (Movie S2). (MPG)

The deformation of MAE film with fixed boundary when the current varies from 0A to 2A and back to 0A (Movie S3). (MPG)

The deformation of MAE film with fixed boundary when the current varies from 0A to 3A and back to 0A (Movie S4). (MPG)

■ AUTHOR INFORMATION

Corresponding Authors

*Tel: +86-0551-63601702. E-mail: xuansh@ustc.edu.cn.

*Tel: +86-0551-63600419. E-mail: gongxl@ustc.edu.cn.

ORCID

Qingchuan Zhang: 0000-0001-8359-3363

Xinglong Gong: 0000-0001-6997-9526

Notes

The authors declare no competing financial interest.

■ ACKNOWLEDGMENTS

Financial support from the National Natural Science Foundation of China (Grant Nos. 11572310 and 11572309) and the Strategic Priority Research Program of the Chinese Academy of Sciences (Grant No. XDB22040502) are gratefully acknowledged. This work is also supported by Collaborative Innovation Center of Suzhou Nano Science and Technology and National Synchrotron Radiation Laboratory (University of Science and Technology of China, KY2090000031).

■ REFERENCES

(1) Nguyen, V. Q.; Ahmed, A. S.; Ramanujan, R. V. Morphing Soft Magnetic Composites. *Adv. Mater.* **2012**, *24*, 4041−54.

(2) Yu, M.; Ju, B.; Fu, J.; Liu, S.; Choi, S.-B. Magnetoresistance Characteristics of Magnetorheological Gel under a Magnetic Field. *Ind. Eng. Chem. Res.* **2014**, *53*, 4704−4710.

(3) Choi, S. B.; Li, W. H.; Yu, M.; Du, H. P.; Fu, J.; Do, P. X. State of the Art of Control Schemes for Smart Systems Featuring Magneto-Rheological Materials. *Smart Mater. Struct.* **2016**, *25*, 043001.

(4) Perales-Martínez, I. A.; Palacios-Pineda, L. M.; Lozano-Sánchez, L. M.; Martínez-Romero, O.; Puente-Cordova, J. G.; Elías-Zúñiga, A. Enhancement of a Magnetorheological PDMS Elastomer with Carbonyl Iron Particles. *Polym. Test.* **2017**, *57*, 78−86.

(5) Li, Y. C.; Li, J. C.; Li, W. H.; Du, H. P. A State-of-the-Art Review on Magnetorheological Elastomer Devices. *Smart Mater. Struct.* **2014**, *23*, 123001.

DOI: 10.1021/acs.iecr.7b04873
Ind. Eng. Chem. Res. 2018, 57, 3246−3254

(6) Sun, S. S.; Yang, J.; Li, W. H.; Du, H.; Alici, G.; Yan, T. H.; Nakano, M. Development of an Isolator Working with Magneto-rheological Elastomers and Fluids. *Mech. Syst. Signal Pr.* **2017**, *83*, 371−384.
(7) Kim, J.; Chung, S. E.; Choi, S. E.; Lee, H.; Kim, J.; Kwon, S. Programming Magnetic Anisotropy in Polymeric Microactuators. *Nat. Mater.* **2011**, *10*, 747−52.
(8) Marchi, S.; Casu, A.; Bertora, F.; Athanassiou, A.; Fragouli, D. Highly Magneto-Responsive Elastomeric Films Created by a Two-Step Fabrication Process. *ACS Appl. Mater. Interfaces* **2015**, *7*, 19112−8.
(9) Lum, G. Z.; Ye, Z.; Dong, X.; Marvi, H.; Erin, O.; Hu, W.; Sitti, M. Shape-Programmable Magnetic Soft Matter. *Proc. Natl. Acad. Sci. U. S. A.* **2016**, *113*, E6007−E6015.
(10) Mishra, S. R.; Dickey, M. D.; Velev, O. D.; Tracy, J. B. Selective and Directional Actuation of Elastomer Films Using Chained Magnetic Nanoparticles. *Nanoscale* **2016**, *8*, 1309−13.
(11) Lazarus, N.; Meyer, C. D.; Bedair, S. S.; Slipher, G. A.; Kierzewski, I. M. Magnetic Elastomers for Stretchable Inductors. *ACS Appl. Mater. Interfaces* **2015**, *7*, 10080−4.
(12) Gao, W.; Wang, L. L.; Wang, X. Z.; Liu, H. Z. Magnetic Driving Flowerlike Soft Platform: Biomimetic Fabrication and External Regulation. *ACS Appl. Mater. Interfaces* **2016**, *8*, 14182−9.
(13) Lee, S.; Yim, C.; Kim, W.; Jeon, S. Magnetorheological Elastomer Films with Tunable Wetting and Adhesion Properties. *ACS Appl. Mater. Interfaces* **2015**, *7*, 19853−6.
(14) Krahn, J.; Bovero, E.; Menon, C. Magnetic Field Switchable Dry Adhesives. *ACS Appl. Mater. Interfaces* **2015**, *7*, 2214−22.
(15) Psarra, E.; Bodelot, L.; Danas, K. Two-Field Surface Pattern Control Via Marginally Stable Magnetorheological Elastomers. *Soft Matter* **2017**, *13*, 6576−6584.
(16) Ramachandran, V.; Bartlett, M. D.; Wissman, J.; Majidi, C. Elastic Instabilities of a Ferroelastomer Beam for Soft Reconfigurable Electronics. *Extreme Mech. Lett.* **2016**, *9*, 282−290.
(17) Rudykh, S.; Bertoldi, K. Stability of Anisotropic Magneto-rheological Elastomers in Finite Deformations: A Micromechanical Approach. *J. Mech. Phys. Solids* **2013**, *61*, 949−967.
(18) Danas, K.; Triantafyllidis, N. Instability of a Magnetoelastic Layer Resting on a Non-Magnetic Substrate. *J. Mech. Phys. Solids* **2014**, *69*, 67−83.
(19) Chen, X.; Xu, X. C.; Ai, S. G.; Chen, H. S.; Pei, Y. M.; Zhou, X. M. Active Acoustic Metamaterials with Tunable Effective Mass Density by Gradient Magnetic Fields. *Appl. Phys. Lett.* **2014**, *105*, 071913.
(20) Guan, X.; Dong, X.; Ou, J. Magnetostrictive Effect of Magnetorheological Elastomer. *J. Magn. Magn. Mater.* **2008**, *320*, 158−163.
(21) Pan, B.; Tian, L.; Song, X. Real-Time, Non-Contact and Targetless Measurement of Vertical Deflection of Bridges Using Off-Axis Digital Image Correlation. *NDT&E Int.* **2016**, *79*, 73−80.
(22) Diaz, J. A.; Moon, R. J.; Youngblood, J. P. Contrast Enhanced Microscopy Digital Image Correlation: A General Method to Contact-Free Coefficient of Thermal Expansion Measurement of Polymer Films. *ACS Appl. Mater. Interfaces* **2014**, *6*, 4856−63.
(23) Früh, A. E.; Artoni, F.; Brighenti, R.; Dalcanale, E. Strain Field Self-Diagnostic Poly(Dimethylsiloxane) Elastomers. *Chem. Mater.* **2017**, *29*, 7450−7457.
(24) Sherafat, M. H.; Guitel, R.; Quaegebeur, N.; Hubert, P.; Lessard, L.; Masson, P. Structural Health Monitoring of a Composite Skin-Stringer Assembly Using within-the-Bond Strategy of Guided Wave Propagation. *Mater. Des.* **2016**, *90*, 787−794.
(25) Brigadnov, I. A.; Dorfmann, A. Mathematical Modeling of Magneto-Sensitive Elastomers. *Int. J. Solids Struct.* **2003**, *40*, 4659−4674.
(26) Galipeau, E.; Rudykh, S.; deBotton, G.; Ponte Castañeda, P. Magnetoactive Elastomers with Periodic and Random Microstructures. *Int. J. Solids Struct.* **2014**, *51*, 3012−3024.
(27) Slesarenko, V.; Rudykh, S. Towards Mechanical Characterization of Soft Digital Materials for Multimaterial 3d-Printing. *Int. J. Eng. Sci.* **2018**, *123*, 62−72.
(28) Goshkoderia, A.; Rudykh, S. Stability of Magnetoactive Composites with Periodic Microstructures Undergoing Finite Strains in the Presence of a Magnetic Field. *Composites, Part B* **2017**, *128*, 19−29.
(29) Boyer, T. H. The Force on a Magnetic Dipole. *Am. J. Phys.* **1988**, *56*, 688−692.
(30) Zhang, Y.; Zhao, X. Wavelet Adaptive Algorithm and Its Application to MRE Noise Control System. *Shock Vib.* **2015**, *2015*, 1−8.

DOI: 10.1021/acs.iecr.7b04873
Ind. Eng. Chem. Res. 2018, 57, 3246−3254